Ruthenium(II) polypyridyl complex as inhibitor of acetylcholinesterase and Aβ aggregation

ARTICLE *in* EUROPEAN JOURNAL OF MEDICINAL CHEMISTRY · JANUARY 2014

Impact Factor: 3.45 · DOI: 10.1016/j.ejmech.2014.01.052 · Source: PubMed

9 AUTHORS, INCLUDING:

Uddhavesh Sonavane
Centre for Development of Advanced Comp…
34 PUBLICATIONS **360** CITATIONS
SEE PROFILE

Vinod Jani
Center for development of advanced comp…
6 PUBLICATIONS **21** CITATIONS
SEE PROFILE

Shefali Ramteke
Agharkar Research Institute
7 PUBLICATIONS **20** CITATIONS
SEE PROFILE

Bimba Joshi
Agharkar Research Institute
21 PUBLICATIONS **593** CITATIONS
SEE PROFILE

European Journal of Medicinal Chemistry 75 (2014) 375–381

Contents lists available at ScienceDirect

European Journal of Medicinal Chemistry

journal homepage: http://www.elsevier.com/locate/ejmech

Original article

Ruthenium(II) polypyridyl complex as inhibitor of acetylcholinesterase and Aβ aggregation

Nilima A. Vyas [a], Satish S. Bhat [a], Avinash S. Kumbhar [a,*], Uddhavesh B. Sonawane [b], Vinod Jani [b], Rajendra R. Joshi [b], Shefali N. Ramteke [c], Prasad P. Kulkarni [c], Bimba Joshi [c]

[a] Department of Chemistry, University of Pune, Pune 411007, India
[b] Bioinformatics Group, Centre for Development of Advanced Computing (C-DAC), University of Pune Campus, Pune 411007, India
[c] Biometry and Nutrition Group, Agharkar Research Institute, Pune 411004, India

ARTICLE INFO

Article history:
Received 13 July 2013
Received in revised form
4 December 2013
Accepted 17 January 2014
Available online 30 January 2014

Keywords:
Ruthenium
Polypyridyl
Inhibition
Acetylcholinesterase
Amyloid-β

ABSTRACT

Two ruthenium(II) polypyridyl complexes $[Ru(phen)_3]^{2+}$ (**1**) and $[Ru(phen)_2(bxbg)]^{2+}$ (**2**) (where phen = 1,10 phenanthroline, bxbg = bis(o-xylene)bipyridine glycoluril) have been evaluated for acetylcholinesterase (AChE) and Amyloid-β peptide (Aβ) aggregation inhibition. Complex **2** exhibits higher potency of AChE inhibition and kinetics and molecular modeling studies indicate that ancillary ligand plays significant role in inhibitory potency exhibited by complex **2**. The inhibitory effect of these complexes on Aβ (1–40) aggregation is investigated using Thioflavin T fluorescence and Transmission Electron Microscopy. Both complexes efficiently inhibit Aβ (1–40) aggregation and are negligibly toxic to human neuroblastoma cells. This is the first demonstration that ruthenium(II) polypyridyl complexes simultaneously inhibit AChE and Aβ aggregation.

1. Introduction

Alzheimer's disease (AD) is the most common form of dementia affecting a large population worldwide. It is a complex neurodegenerative condition in which several molecular dysfunctions result in formation and deposition of β-amyloid peptides (Aβ) in brain, τ-protein aggregation, oxidative stress and cholinergic neuronal loss [1,2]. Cholinergic strategy of prolonging acetylcholine existence in synapses by using acetylcholinesterase (AChE) inhibitors is a leading strategy as most of the marketed drugs for AD, such as tacrine, donepezil, rivastigmine, and galantamine are AChE inhibitors [3]. However due to complex and multifactorial nature of AD, a new strategy of targeting more than one target by a single drug candidate viz. multi-target-directed ligands (MTDLs) strategy is emerging for AD drug design [4,5].

Acetylcholinesterase functions in nerve transmission and rapidly hydrolyzes acetylcholine into acetate and choline in cholinergic synapses. Catalytic Active Site (CAS) of AChE has an unusual location at the bottom of a deep narrow gorge lined with several aromatic amino acid residues and a Peripheral Anionic Site (PAS) is located at the entrance [6]. It has been found that, apart from the vital role in nerve transmission, AChE also plays an important but a non-classical role, in processing of Aβ peptides, a major neuropathological hallmark of AD [7,8]. PAS of AChE is involved in the acceleration of Aβ aggregation [9]. Aβ aggregates are insoluble senile plaques which are highly toxic to neurons and considered as promising target for AD treatment [1,2]. Dual functional AChE inhibitors that can bind to both CAS and PAS are of current interest as they can simultaneously inhibit AChE activity and delay Aβ aggregation [4]. Following this rationale, dual binding AChE inhibitors have been successfully designed exhibiting higher potency than single site inhibitors from which they have been derived [10–12]. Moreover many of these hybrids are also potent inhibitors of Aβ aggregation highlighting their MTDL property [13–15].

Ruthenium polypyridyl complexes find extensive biological applications in design of DNA structure probes, diagnostic and imaging agents [16,17]. Recently Eric Meggers and coworkers designed metal complex scaffolds as enzyme inhibitors using bioactive enzyme specific ligands evidencing the potential applications of octahedral metal complexes in drug design [18–20]. AChE inhibition by metal complexes has been restricted to antitumor cis-platin [21], metal porphyrin [22], metal amine complexes [23] and few cationic ruthenium polypyridyl complexes [24]. Ruthenium polypyridyl complexes though known for a long time as inhibitors of AChE [24],

* Corresponding author. Fax: +91 020 25691728.
E-mail address: askum@chem.unipune.ac.in (A.S. Kumbhar).

0223-5234/$ – see front matter © 2014 Elsevier Masson SAS. All rights reserved.
http://dx.doi.org/10.1016/j.ejmech.2014.01.052

are still unexploited. Eric Meggers and coworkers have reported tris-heteroleptic polypyridyl ruthenium(II) complex as nanomolar AChE inhibitor [25], which is 50 times more potent than the parent $[Ru(phen)_3]^{2+}$ (**1**) (where phen = 1,10 phenanthroline), however the detailed kinetic analysis of inhibition nor the mode of binding is reported.

Ruthenium polypyridyl complexes offer several advantages like feasible synthesis, inertness to substitution, stability in biological environment, expansions of functional groups by variation in surrounding ligands and inherent photophysical properties. In this work we report ruthenium(II) polypyridyl complex $[Ru(phen)_2(bxbg)]^{2+}$ (**2**) (where bxbg = bis(o-xylene)bipyridine glycoluril) with MTDL potential in which one phenanthroline ligand in parent complex **1** has been modified to provide both enhanced AChE inhibition and Aβ aggregation inhibition (Fig. 1). To the best of our knowledge these are the first examples of ruthenium(II) polypyridyl complexes wherein their AChE inhibition kinetics has been evaluated and corroborated by molecular modeling studies and their anti-Aβ aggregation potential has also been explored.

2. Results and discussion

2.1. AChE inhibition

The complex **2** was synthesized and characterized as reported [26] and evaluated as inhibitor of AChE (*Electrophorus electricus*) following the method of Ellman [27]. The preliminary studies by UV–Visible and fluorescence spectroscopy indicated binding of complexes with AChE (Figs. S1 and S2 in supporting information). As a positive control previously known ruthenium complex $[Ru(phen)_3]^{2+}$ (**1**) [24] is used. Propidium iodide is a well known PAS binder [28] and is used as standard for AChE inhibition studies. AChE inhibition data for complexes **1** and **2** along with propidium iodide is given in Table 1. IC_{50} values for propidium iodide (IC_{50} = 11.13 ± 1.0 μM) and complex **1** (IC_{50} = 9.23 ± 0.6 μM) are nearly same while complex **2** inhibits AChE with IC_{50} value 0.30 ± 0.02 μM. Compared with **1** complex **2** is 30-fold more potent AChE inhibitor (Fig. 2). The presence of benzene rings in complex **2** in modified phenanthroline ligand improved its inhibition potency.

The detailed kinetic analysis of binding of complexes with AChE was studied. An analysis of Lineweaver–Burk reciprocal plots for **1** showed decrease in V_{max} with increase in inhibitor concentration with constant K_m (Fig. 3) indicating a non-competitive mode of inhibition. Complex **2** shows mixed type of inhibition with decreased V_{max} and increased K_m with higher inhibitor concentration as shown in Fig. 4. Significant lower value of inhibition constant (K_i = 0.04 μM) indicates strong binding of complex to AChE. The non-competitive inhibition observed for **1** is similar to propidium iodide (Fig. S3 in supporting information) which is a well known AChE inhibitor that binds exclusively at PAS. Whereas inhibition property of complex **2** closely resembles to tacrine, tacrine heterodimers and heterodimers of propidium which bind at both catalytic and peripheral sites of AChE [5,29].

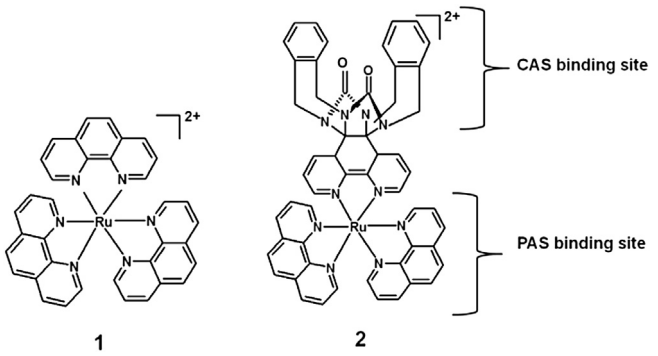

Fig. 1. Ruthenium polypyridyl complexes as AChE inhibitors used in the present study.

Table 1
AChE inhibition data of **1**, **2** and propidium iodide.

Compound	IC_{50} ± SD (μM)[a]	K_i[b] ± SD (μM)[a]	Type of inhibition
1	9.23 ± 0.6	4.1 ± 0.6	Non-competitive
2	0.30 ± 0.02	0.04 ± 0.04	Mixed
Propidium iodide	11.13 ± 1.0	7.8 ± 1.8	Non-competitive

[a] Mean ± SD for three different experiments.
[b] Estimates of K_i were obtained from replots of the slopes of Lineweaver–Burk plots vs inhibitor concentration.

2.2. Molecular modeling studies

Molecular docking experiments were carried out to determine the orientation of these complexes within the active gorge of the AChE. According to internal energies of binding affinities and grid scores (Table S1 in supporting information), surface views of top scored positions of **1** and **2** are shown in Fig. 5. The active site of the gorge is highlighted by yellow color and PAS by red. Complex **1** prefers binding with PAS and midgorge amino acids (Fig. 5-a) whereas complex **2** enters the gorge and interacts with PAS, CAS and midgorge amino acids (Fig. 5-b) confirming the results of kinetic studies.

Molecular interactions of complex **1** with AChE (Fig. 6-a) show partial π–π stacking interactions of phenanthrolines with Trp279 and Tyr70 residues of PAS and also with Tyr121 and Tyr334 residues in the midgorge region. These results indicate that binding pattern of complex **1** with AChE is similar to the one reported for propidium iodide [28,30]. In contrast, complex **2** fits perfectly in the active gorge of AChE interacting with residues encompassing CAS, PAS and midgorge regions (Fig. 6-b). Entry of rigid and bulky bxbg ligand in the narrow active gorge may follow a similar way of enzyme breathing by which large and rigid CAS binding AChE inhibitors such as huperzine A, galanthamine and also AChE substrate acetylcholine (ACh) having diameter higher than the bottleneck of gorge enter the gorge [31]. Two benzene rings of bxbg firmly bind to catalytic triad amino acids (Glu327, His440, Ser200), Ser200 being stacked exactly between the two rings. Ser200 forms cation–

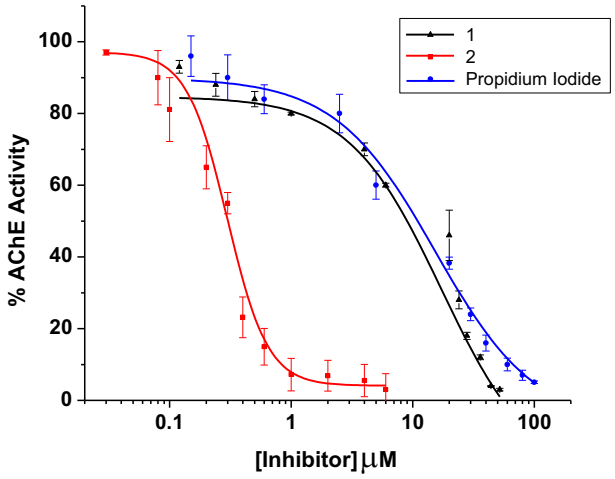

Fig. 2. IC_{50} curves against AChE of the complexes **1**, **2** and propidium iodide. (Complexes are racemic).

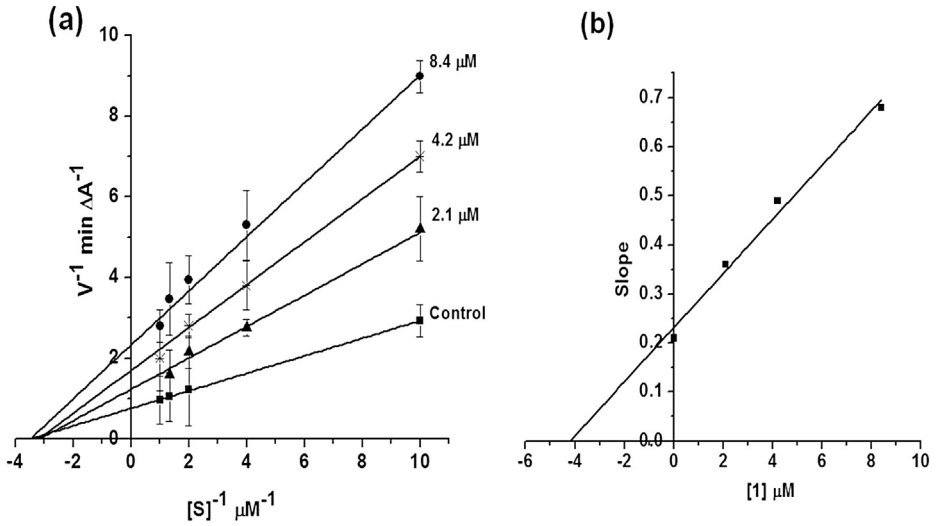

Fig. 3. Steady state inhibition of AChE hydrolysis of acetylthiocholine (ATCh) by **1**. (a) Lineweaver–Burk reciprocal plots of initial velocity and substrate concentration (0.1–1.0 mM) show non-competitive inhibition. (b) Replot of the slopes of reciprocal plots vs inhibitor concentration for estimation of K_i. The *x* axis intercept represents the K_i of the inhibitor.

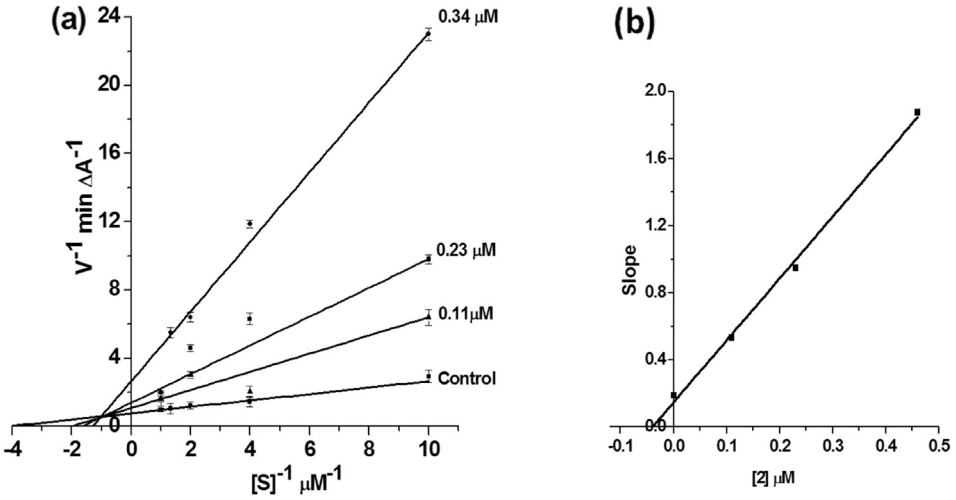

Fig. 4. Steady state inhibition of AChE hydrolysis of acetylthiocholine (ATCh) by **2**. (a) Lineweaver–Burk reciprocal plots of initial velocity and substrate concentration (0.1–1.0 mM) show mixed type of inhibition. (b) Replot of the slopes of reciprocal plots vs inhibitor concentration for estimation of K_i. The *x* axis intercept represents the K_i of the inhibitor.

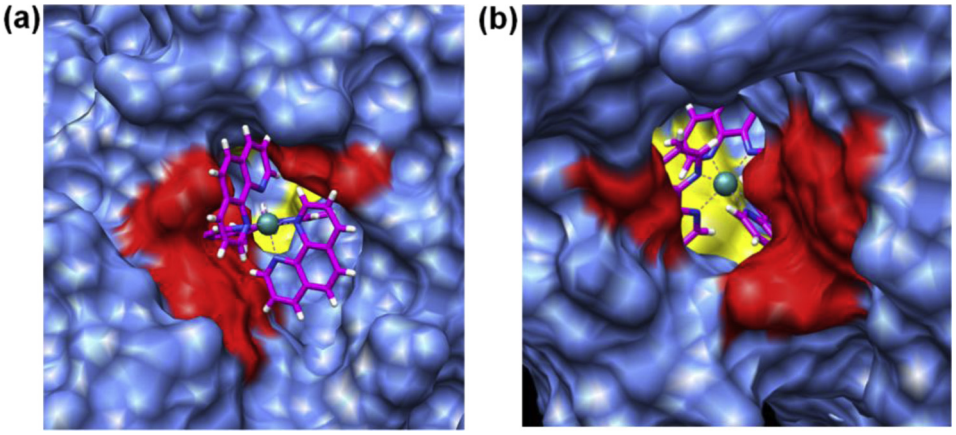

Fig. 5. Top scored positions of **1** and **2** (magenta) in AChE active site (PDB id 1QTI). PAS region and internal gorge with catalytic site of the enzyme are highlighted in red and yellow respectively. (a) Top-scored docking pose of **1** in AChE shows PAS binding of **1**. (b) Top-scored docking pose of **2** in AChE shows binding at CAS and PAS.

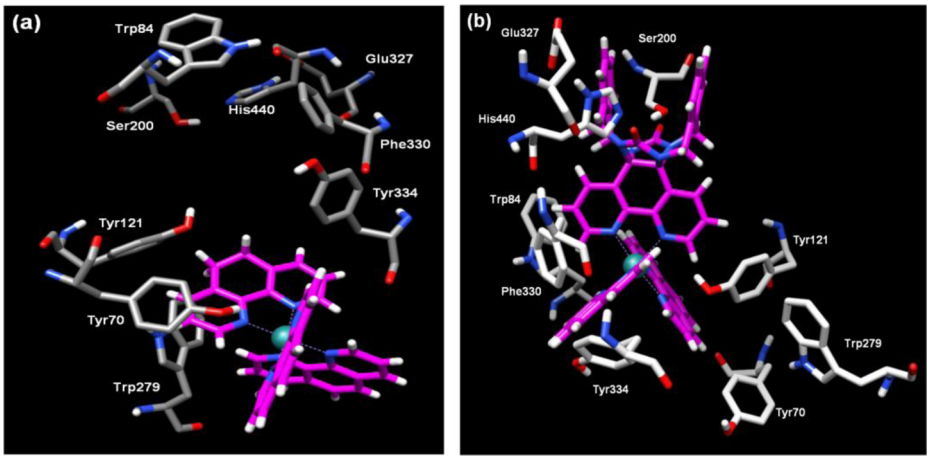

Fig. 6. Representation of the complexes **1**(a) and **2**(b) (magenta) (and all other atoms are colored by atom type) docked into the binding site of AChE highlighting key amino acids of the active gorge.

π interaction with both benzene rings. One oxygen from glycoluril functionality is hydrogen bonded to N–H group of Ala201 (O–H distance$_{average}$ 2.3 Å). His440 exhibits π–π interaction with one of the benzenes and also cation–π with one C=O group of bxbg ligand. Apart from catalytic triad, several amino acids from the active gorge interact with bxbg ligand by weak electrostatic interactions. (Fig. S4 in supporting information shows detail view of these interactions). Full or partial overlap of aromatic rings Trp84 of CAS, Tyr334, Phe330, Tyr121 of midgorge and Tyr70, Trp279 of PAS with all three phenanthroline moieties plays active role in high inhibitory potency displayed by complex **2**.

The Root Mean Square Deviation (RMSD) for key amino acids involved in binding interactions determined by Molecular Dynamics (MD) simulations (Fig. S5 in supporting information) is fairly stable for 5ns evidencing that the complex **2** is dynamically stable in AChE active gorge. Positively charged ruthenium complex also plays a considerable role by interacting with midgorge Lys118, Ser122, Tyr121 and Trp84 by weak electrostatic and cation–π interactions.

2.3. *Aβ aggregation inhibition*

We further studied the inhibitory effect of complexes **1** and **2** on Aβ aggregation by Thioflavin T (ThT) fluorescent method [32]. In the control experiment, 42 μM Aβ(1–40) aggregation reaches maxima at around 144 h. In the presence of **1** at 1:1 M ratio, the aggregation starts at 100 h of incubation and at the end of 200 h, only 20% aggregation is observed. On the other hand complex **2** completely inhibited aggregation up to 200 h (Fig. 7).

Transmission electron microscopy (TEM) results (Fig. 8a–c) were consistent with the ThT results. Control Aβ(1–40) resulted in dense, thick and large fibril formation in 10 days, whereas addition of complex **1** results in fewer but long fibrils indicating delayed nucleation process. In case of complex **2** both the number and length of fibrils is significantly reduced. In case of complex **2** the functionalized ligand may be involved in hydrogen bonding interactions with Aβ peptide in addition to the π–π interactions and hydrophobic interactions similar to those observed for binding of $[Ru(bpy)_2dppz]^{2+}$ [33] (where bpy is 2,2′-bipyridine; dppz = dipyrido[3,2-a:2′-,3′-c]-phenazine) and phenanthroline based Pt(II) complexes to Aβ [34].

2.4. *Cytotoxicity studies*

Majority of ruthenium polypyridyl complexes investigated for their medicinal applications are coordinatively saturated and substitutionally inert and exhibit antiproliferative activity due to their noncovalent DNA binding [17]. However, there are, exceptions in which ruthenium polypyridyl complexes exhibit very low toxicity and have been used for the different medicinal application apart from the well studied antitumor activity [35,36]. Cytotoxicity of complexes **1** and **2** towards human neuroblastoma cells SH-SY5Y was carried out by MTT assay. This cell line is an appropriate model to study neurotoxic effect of drugs [37] and various organic acetylcholinesterase inhibitors have been tested for their neurotoxic effect using this cell line [38,39]. In the presence of complexes at 40 μM concentration, cell viability after 24 h is above 95% (Fig. 9). This complex concentration is used for Aβ aggregation inhibition studies which is also significantly higher than their IC_{50} values of AChE inhibition and toxicity of complexes is negligible under biological conditions. Cytotoxicity and AChE inhibition results indicate that complex **2** can be used as potential AChE inhibitor. Further studies in this direction are underway in our laboratory.

3. Conclusion

In summary we have reported for the first time the simultaneous inhibition of AChE and Aβ aggregation by nontoxic ruthenium(II) polypyridyl complexes. For metal complexes of

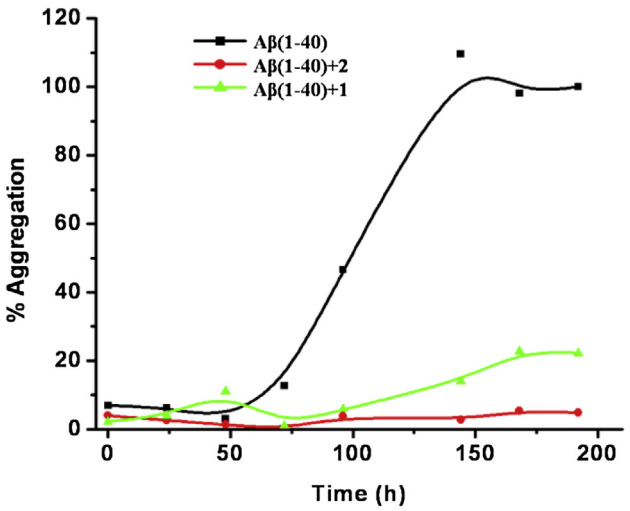

Fig. 7. Inhibition of Aβ(1–40) aggregation by complexes **1** and **2** monitored by ThT fluorescence. Aβ(1–40): Complex ratio used was 1:1 (42 μM).

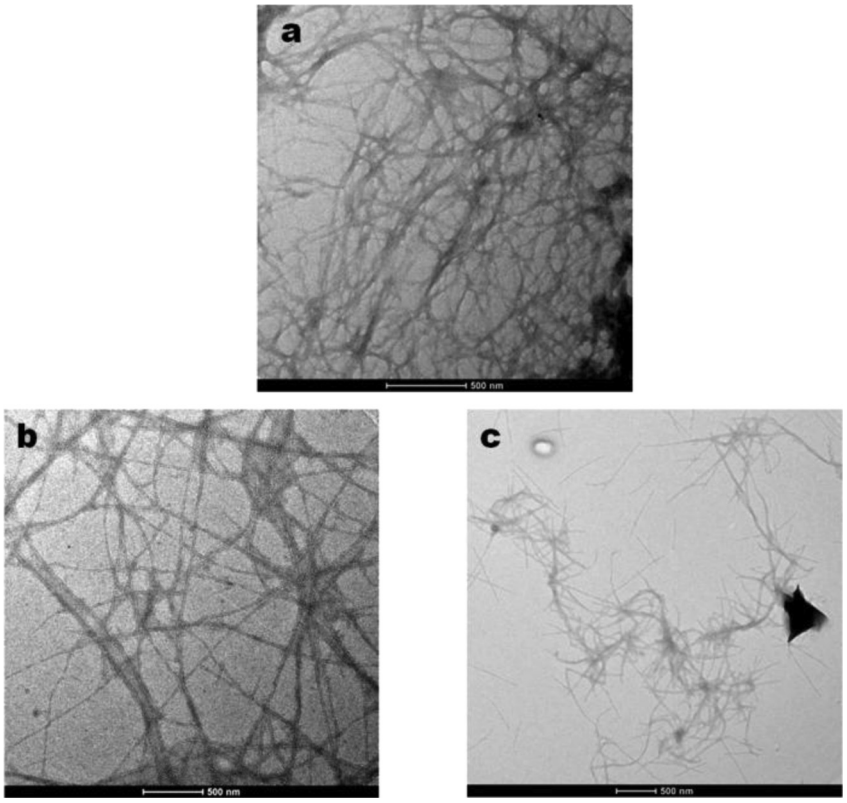

Fig. 8. TEM images of Aβ(1–40) after 10 days of incubation alone (a) and in presence of **1**(b) and **2**(c) at 37 °C, pH 7.0, Aβ(1–40): Complex ratio used was 1:1 (42 μM).

polypyridyl ligands, considering advantage of stability, inertness and diverse availability of modification, such MTDL strategy can be adopted for developing metal based therapy for AD.

4. Experimental

4.1. Materials

All reagents and solvents were purchased commercially and were used as received. Acetylcholinesterase from *Electrophoricus electricus* (*Ee*AChE) Type V–S, acetylthiocholine iodide, 5,5′-dithiobis(2-nitrobenzoic) acid (DTNB), propidium iodide, human Amyloid-β peptide (1–40), 1,1,1,3,3,3-hexafluoro-2-propanol (HFIP) and Thioflavin T (ThT) were purchased from Sigma–Aldrich. 3-(4,5-dimethylthiazol-2-yl)-2,5-diphenyltetrazolium bromide (MTT) was purchased from Spectrochem Pvt. Ltd., Mumbai. Dulbecco's Modified Eagle Medium (DMEM), Fetal Bovine Serum (FBS), Phosphate Buffered Saline for cell culture were purchased from HiMedia, Mumbai.

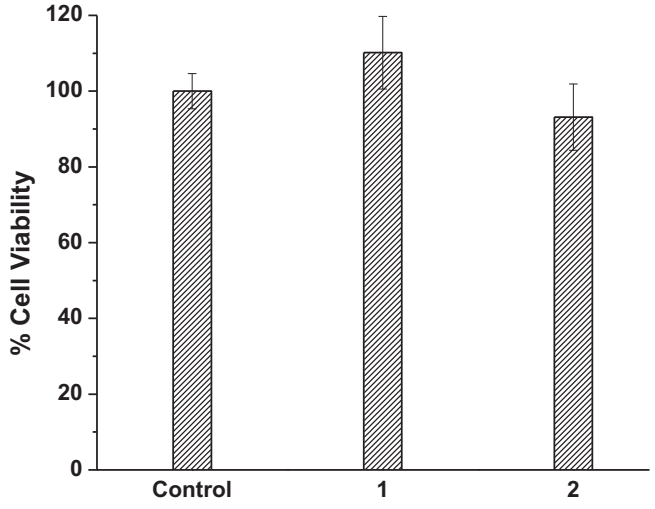

Fig. 9. Cytotoxicity evaluation of complexes **1** and **2** against neuroblastoma cell line SH-SY5Y. The cell viability was measured after 24 h by MTT assay. Each data point represents the mean for three different experiments.

4.2. Methods and instrumentation

UV–Visible spectra were recorded on a Jasco UV–vis spectrophotometer. The concentration of AChE solution in 10 mM phosphate buffer of pH 7.0 was calculated from its known extinction coefficient at 280 nm (Extinction Coefficient: $E^{1\%} = 18.0$). Absorbance measurements for enzyme assay were performed on a Thermo-Fischer Multiskan FC plate reader. Steady state fluorescence measurements were recorded on Shimadzu RF-5301 spectrofluorometer at room temperature. Microscopy images were captured on Technai G^2 20 Ultra Twin, FEI transmission electron microscope at Department of Physics, University of Pune.

4.3. Acetylcholinesterase-inhibitor interaction by UV–visible spectroscopy

Increments of aliquots of 10 μL of 2.6 μM AChE in phosphate buffer pH = 7.0 were added to 10 μM of inhibitor in phosphate buffer pH = 7.0. Changes in absorption were monitored. Blanks containing no inhibitors were also run.

4.4. Acetylcholinesterase tryptophan fluorescence quenching assay

To a solution of 100 nm enzyme solution in phosphate buffer pH = 7.0 increments of complex **2** were added to obtain

concentration range as 0–50 μM. Tryptophan fluorescence was monitored at 340 nm (λ_{ex} = 280 nm).

4.5. Acetylcholinesterase inhibition

Acetylcholinesterase(AChE) inhibitory activity of complexes was evaluated spectrophotometrically by the method of Ellman [27] using purified AChE from *E. electricus* (type V–S) and acetylthiocholine iodide as substrate. Stock solutions of tested complexes (racemic mixture) were prepared in dimethyl sulfoxide (DMSO) which were diluted with phosphate buffer of pH 7.0 to give final DMSO concentration of 0.15% in the assay reaction mixture. This DMSO concentration did not affect AChE activity. The reaction took place in a final volume of 200 μL of 0.1 M phosphate-buffered solution, pH 8.0, containing 20 μL AChE (0.47 U/ml in 10 mM phosphate buffer of pH 7.0), 20 μL of a 3.3 mM solution of 5,5′-dithiobis(2-nitrobenzoic) acid (DTNB) in 10 mM phosphate buffer of pH 7.0 containing 6 mM $NaHCO_3$ and 20 μL of a solution of inhibitor (ten to twelve concentrations ranging from 0.001 μM to 100 μM). After 20 min incubation period at 25 °C, 20 μL of acetylthiocholine iodide (3.0 mM aqueous solution) was added. Hydrolysis of substrate was followed by measuring the variation of the absorbance at 405 nm for 5 min. Self hydrolysis of substrate was verified by running a blank containing no inhibitor and no enzyme in the reaction mixture. Inhibitor controls were also run separately under the same conditions to eliminate inhibitor contribution in the readings. IC_{50} value that is concentration of inhibitor that reduces 50% enzyme activity was calculated by nonlinear regression of the response-log (concentration) curve. Data are expressed as the mean ± SD of at least three different experiments in triplicate.

4.6. Kinetic analysis of the AChE inhibition

To obtain estimates of mechanism of action of these compounds reciprocal plots of 1/V vs 1/[S] were constructed at different substrate concentrations (0.1–1 mM) by the method of Ellman. Final reaction mixture volume 200 μL (0.1 M phosphate-buffered solution, pH 8.0) contained 20 μL of enzyme (0.47 U/ml in 10 mM phosphate buffer of pH 7.0), 20 μL of a 3.3 mM solution of 5,5′-dithiobis(2-nitrobenzoic) acid (DTNB) and 20 μL of inhibitor to give final desired concentration. Progress curves were monitored at 405 nm for 3 min with and without inhibitor concentrations. The plots were assessed by a weighted least-squares analysis. Slopes of the reciprocal plots were plotted against inhibitor concentration for the estimation of K_i, as the *x*-axis intercept.

4.7. Molecular docking

The molecular docking studies were carried out using crystal structure coordinates of AChE from *Torpedo californica* (*Tc*AChE) PDB ID 1QTI. The crystal structure of *Tc*AChE is used due to its similarity to *Ee*AChE sequence. Amber ff99SB force field was applied to parameterize protein. All water molecules are removed. Protein preparation was carried out using chimera software [40]. Ruthenium complexes were docked into active site of enzyme. Prior to docking the ruthenium complexes were energy optimized through DFT method using gaussian03 [41]. The partial atomic charges for the compounds were derived using Guassian 03 program package using Becke's three parameter hybrid functional (B3LYP) method and LANL2DZ basis set for the ruthenium atom and 6–31G(d,p) basis set for the other atoms. Docking was carried out using DOCK6 software [42]. The reliability of this was accessed by docking a known tacrine based dual AChE inhibitor (PDB entry 2CMF). Each compound was subjected to multiple docking runs. Analyses of docking results were carried out using chimera by visual inspection along with the docking scores. Rigid docking was carried for these complexes. The relative binding affinities of the best poses of the complexes were determined by using gridscore.

Further, molecular dynamics simulations were run using the AMBER 11 suite of program for complex **2**-AChE system to check the stability of binding mode obtained by docking. Protein-**2** complex was subjected to a short minimization of 5000 steps comprising of initial 2500 steps of steepest descent and remaining 2500 steps of conjugate gradient. This minimized structure was further heated till 300 K and then equilibrated for 1ns at the same temperature. The equilibrated structure was then subjected to production run for 5 ns. Protein was allowed to move with **2** restrained. Root Mean Square Deviation (RMSD) for the residues belonging to CAS and PAS region are calculated by "ptraj" module of AMBER.

4.8. Inhibition of Aβ(1–40) aggregation: Thioflavin T assay

Lyophilized Aβ (1–40) was dissolved in HFIP and stored at −80 °C. For aggregation experiments, HFIP was removed using a speed-vac system and the peptide/HFIP films were redissolved in 200 μl dimethyl sulfoxide (DMSO). Immediately thereafter, the Aβ peptide solutions were separated from the DMSO by means of a desalting column (HiTrap™ Desalting column (cat. 17-1408-01), GE Healthcare) that was pre-equilibrated with 25 ml PBS buffer, pH 7.4. The 200 μl sample was applied to the column using a 1 ml syringe followed by additional injection of 1.5 ml buffer. Fractions of 500 μl each were collected and the peptide concentration was determined using the BCA protein estimation assay.

Aggregate-free Aβ(1–40) solutions at a final concentration of 42 μM were prepared as described above. Aggregation in the presence of complexes was recorded by the addition of the respective complex at a final concentration of 42 μM. The samples were incubated at 37 °C in PBS pH 7.4. Amyloid beta aggregation was monitored by Thioflavin T (ThT) fluorescence method [32]. Periodically, aliquots of 20 μL from assay mixture were removed and diluted with 1X PBS containing 40 μM ThT to a final volume of 500 μL. Fluorescence readings were recorded every 24 h for a period of 10 days. The fluorescence was measured (λ_{ex} = 430 nm and λ_{em} = 490 nm) using a FL-2500 Hitachi fluorescence spectrophotometer. At the concentrations tested and parameters used, ruthenium complexes exhibited no fluorescence alone and also in presence of ThT.

4.9. Inhibition of Aβ(1–40) aggregation: TEM study

For TEM analysis samples prepared for ThT assay were used after 10 days of incubation. Aliquots of 10 μL of samples were placed on a carbon-coated copper grid. After drying, the specimen was examined under a Technai G^2 20 Ultra Twin, FEI transmission electron microscope working at 200 kV.

4.10. Cytotoxicity studies

Human neuroblastoma cells SH-SY5Y were grown in DMEM & Ham's F-12 medium supplemented with 10% fetal bovine serum (FBS) and 1% antibiotic solution (penicillin & streptomycin) at 37 °C in humidified chamber under 5% CO_2. The compound solutions (40 μM in Phosphate buffer of pH 7.0 containing 1% DMSO) were passed through 0.22 μm syringe filters for sterilization before treatment. Cell viability was measured in 96-well plates by quantitative colorimetric assay using MTT. Briefly, 10^5 cells per ml were seeded in 96-well plates for assay. The cells were treated with compounds in media without FBS. At 24 h after the treatment, media was removed and MTT was added to the wells at the final

concentration as 5 mg/ml and the cells were incubated at 37 °C for another 3 h. The MTT solution was removed and the colored formazan crystals in each well were dissolved in 150 μL dimethyl sulfoxide. Absorbance at 595 nm was measured using a μQuant, Biotek Instruments microplate reader.

Acknowledgments

NAV acknowledges Department of Science and Technology (DST), India, (SR/WOS-A/CS-63/2010). ASK acknowledges DST (SR/S5/BC-25/2006) and UGC (F. No. 32-198/2006(SR)) for funding. Authors thank DST (FIST, PURSE) and UGC (CAS) funding to the Department of Chemistry. We thank Dr. A. Ravikumar and S. Ponnusamy, for providing plate reader facility and useful suggestions and Shridharkrishna for TEM measurements. UBS and VJ acknowledge 'Bioinformatics Resources and Applications Facility' (BRAF) for providing the computational facility. PPK acknowledges DST (SR/S1/IC-03/2010) and Department of Biotechnology, India (BT/PR3871/MED/30/830/2012) for funding. SNR thanks UGC, India for J.R.F. (F. No. 20-12/2009).

Appendix A. Supplementary data

Supplementary data related to this article can be found at http://dx.doi.org/10.1016/j.ejmech.2014.01.052.

References

[1] E.D. Roberson, L. Mucke, Science 314 (2006) 781–784.
[2] M. Goedert, M.G. Spillantini, Science 314 (2006) 779–781.
[3] W.H. Suh, K.S. Suslick, Y.-H. Suh, Curr. Med. Chem. CNS Agents 5 (2005) 259–269.
[4] A. Cavalli, M.L. Bolognesi, A. Minarini, M. Rosini, V. Tumiatti, M. Recanatini, C. Melchiorre, J. Med. Chem. 51 (2008) 347–372.
[5] S. Rizzo, A. Bisi, M. Bartolini, F. Mancini, F. Belluti, S. Gobbi, V. Andrisano, A. Rampa, Eur. J. Med. Chem. 46 (2011) 4336–4343.
[6] D.M. Quinn, Chem. Rev. 87 (1987) 955–979.
[7] I. Silman, J.L. Sussman, Curr. Opin. Pharma. 5 (2005) 293–302.
[8] A. Alvarez, R. Alarcon, C. Opazo, E.O. Campos, F.J. Munoz, F.H. Calderon, F. Dajas, M.K. Gentry, B.P. Doctor, F.G. De Mello, N.C. Inestrosa, J. Neurosci. 18 (1998) 3213–3223.
[9] N.C. Inestrosa, A. Alvarez, C.A. Perez, R.D. Moreno, M. Vicente, C. Linker, O.I. Casanueva, C. Soto, C.J. Garrido, Neuron 16 (1996) 881–891.
[10] P. Camps, X. Formosa, D. Munõz-Torrero, J. Petrignet, A. Badia, M.V. Clos, J. Med. Chem. 48 (2005) 1701–1704.
[11] O.J. Bornstein, T.J. Eckroat, J.L. Houghton, C.K. Jones, K.D. Green, S. Garneau-Tsodikova, Med. Chem. Commun. 2 (2011) 406–412.
[12] P.W. Elsinghorst, J.S. Cieslik, K. Mohr, C. Tränkle, M. Gütschow, J. Med. Chem. 50 (2007) 5685–5695.
[13] M.L. Bolognesi, M. Bartolini, F. Mancini, G. Chiriano, L. Ceccarini, M. Rosini, A. Milelli, V. Tumiatti, V. Andrisano, C. Melchiorre, ChemMedChem 5 (2010) 1215–1220.
[14] M. Catto, A. Berezin, D.L. Re, G. Loizou, M. Demetriades, A.D. Stradis, F. Campagna, P.A. Koutentis, A. Carotti, Eur. J. Med. Chem. 58 (2012) 84–97.
[15] L. Piazzi, A. Rampa, A. Bisi, S. Gobbi, F. Belluti, A. Cavalli, M. Bartolini, V. Andrisano, P. Valenti, M. Recanatini, J. Med. Chem. 46 (2003) 2279–2282.
[16] K.E. Erkkila, D.T. Odom, J.K. Barton, Chem. Rev. 99 (1999) 2777–2795.
[17] M.R. Gill, J.A. Thomas, Chem. Soc. Rev. 41 (2012) 3179–3192.
[18] H. Bregman, P.J. Carroll, E. Meggers, J. Am. Chem. Soc. 128 (2006) 877–884.
[19] E. Meggers, Chem. Commun. (2009) 1001–1010.
[20] E. Meggers, Angew. Chem. Int. Ed. 50 (2011) 2442–2448.
[21] M.A. Kamala, F.H. Nasimb, A.A. Al-Jafaria, Cancer Lett. 138 (1999) 115–119.
[22] B.H. Lee, M.B. Park, B.S. Yu, Bioorg. Med. Chem. Lett. 8 (1998) 1467–1470.
[23] E. Mario, S.J. Bolton, Pharm. Sci. 57 (1968) 418–422.
[24] F.P. Dwyer, E.C. Gyarfas, W.P. Rogers, J.H. Koch, Nature 170 (1952) 190–191.
[25] S.P. Mulcahy, S. Li, R. Korn, X. Xie, E. Meggers, Inorg. Chem. 47 (2008) 5030–5032.
[26] S.S. Bhat, A.S. Kumbhar, P. Lönnecke, E. Hey-Hawkins, Inorg. Chem. 49 (2010) 4843–4853.
[27] G.L. Ellmann, D. Courtney, V. Andres Jr., R.M. Featherstone, Biochem. Pharmacol. 7 (1961) 88–95.
[28] Y. Bourne, P. Taylor, Z. Radić, P. Marchot, EMBO J. 22 (2003) 1–12.
[29] W. Luo, Y.-P. Li, Y. He, S.-L. Huang, D. Li, L.-Q. Gu, Z.-S. Huang, Eur. J. Med. Chem. 46 (2011) 2609–2616.
[30] A. Cavalli, G. Bottegoni, C. Raco, M. De Vivo, M. Recanatini, J. Med. Chem. 47 (2004) 3991–3999.
[31] I. Silman, J.L. Sussman, Chem. Biol. Interact. 175 (2008) 3–10.
[32] H. Levine III, Protein Sci. 2 (1993) 404–410.
[33] N.P. Cook, M. Ozbil, C. Katsampes, R. Prabhakar, A.A. Martí, J. Am. Chem. Soc. 135 (2013) 10810–10816.
[34] G. Ma, F. Huang, X. Pu, L. Jia, T. Jiang, L. Li, Y. Liu, Chem. Eur. J. 17 (2011) 11657–11666.
[35] S.S. Bhat, A.S. Kumbhar, A.A. Kumbhar, A. Khan, A.P. Lönnecke, E. Hey-Hawkins, Chem. Commun. 47 (2011) 11068–11070.
[36] E. Musatkina, H. Amouri, M. Lamoureux, T. Chepurnykh, C. Cordier, J. Inorg. Biochem 101 (2007) 1086–1089.
[37] G. Nicolini, M. Miloso, C. Zoia, A. Di Silvestro, G. Cavaletti, G. Tredici, Anticancer Res. 18 (1998) 2477–2481.
[38] G.C. González-Muñoz, M.P. Arce, B. López, C. Pérez, M. Villarroya, M.G. López, A.G. García, S. Conde, M.I. Rodríguez-Franco, Eur. J. Med. Chem. 45 (2010) 6152–6158.
[39] T. Mohamed, X. Zhao, L.K. Habib, J. Yang, P.P.N. Rao, Bioorg. Med. Chem. 19 (2011) 2269–2281.
[40] E.F. Pettersen, T.D. Goddard, C.C. Huang, G.S. Couch, D.M. Greenblatt, E.C. Meng, T.E. Ferrin, J. Comput. Chem. 13 (2004) 1605–1612.
[41] M.J. Frisch, G.W. Trucks, H.B. Schlegel, G.E. Scuseria, M.A. Robb, J.R. Cheeseman, J.A. Montgomery Jr., T. Vreven, K.N. Kudin, J.C. Burant, J.M. Millam, S.S. Iyengar, J. Tomasi, V. Barone, B. Mennucci, M. Cossi, G. Scalmani, N. Rega, G.A. Petersson, H. Nakatsuji, M. Hada, M. Ehara, K. Toyota, R. Fukuda, J. Hasegawa, M. Ishida, T. Nakajima, Y. Honda, O. Kitao, H. Nakai, M. Klene, X. Li, J.E. Knox, H.P. Hratchian, J.B. Cross, C. Adamo, J. Jaramillo, R. Gomperts, R.E. Stratmann, O. Yazyev, A.J. Austin, R. Cammi, C. Pomelli, J.W. Ochterski, P.Y. Ayala, K. Morokuma, G.A. Voth, P. Salvador, J.J. Dannenberg, V.G. Zakrzewski, S. Dapprich, A.D. Daniels, M.C. Strain, O. Farkas, D.K. Malick, A.D. Rabuck, K. Raghavachari, J.B. Foresman, J.V. Ortiz, Q. Cui, A.G. Baboul, S. Clifford, J. Cioslowski, B.B. Stefanov, G. Liu, A. Liashenko, P. Piskorz, I. Komaromi, R.L. Martin, D.J. Fox, T. Keith, M.A. Al-Laham, C.Y. Peng, A. Nanayakkara, M. Challacombe, P.M.W. Gill, B. Johnson, W. Chen, M.W. Wong, C. Gonzalez, J.A. Pople, Gaussian 03, Revision C.02, Gaussian, Inc, Pittsburgh PA, 2003.
[42] D.T. Moustakas, P.T. Lang, S. Pegg, E.T. Pettersen, I.D. Kuntz, N. Broojimans, R.C. Rizzo, J. Comput. Aided Mol. Des. 20 (2006) 601–609.